$^{13}C-^{1}H$ and $^{13}C-^{13}C$ Spin Coupling Behavior in Aldofuranosyl Rings from Density Functional Theory

Francis Cloran,[†] Ian Carmichael,*[,‡] and Anthony S. Serianni*[,†]

Department of Chemistry and Biochemistry and Radiation Laboratory, University of Notre Dame, Notre Dame, Indiana 46556

Received: February 16, 1999

Ab initio molecular orbital calculations using density functional theory (DFT) have been conducted on the aldopentofuranose, 2-deoxy-β-D-*erythro*-pentofuranose (**1**) to evaluate the performance of DFT methodology in structural optimization and NMR spin−spin coupling constant determinations prior to its application in more complex carbohydrate-containing systems. Computed molecular parameters (bond lengths, bond angles, bond torsions) and NMR spin−spin coupling constants (J) in the 10 geometrically optimized envelope forms of **1** are compared to those reported previously from HF/6-31G*-optimized geometries. In earlier work, $^{n}J_{CH}$ values were first computed at the HF level using finite-field perturbation theory and a basis set specially designed to economically recover the Fermi-contact contribution to J. Electron correlation effects on the coupling constants were then introduced via second-order Møller−Plesset perturbation (MP2) calculations. The derived correlation corrections (i.e., the MP2 − HF values) were scaled by factors obtained from more elaborate quadratic configuration interaction (QCISD) calculations on related, though necessarily smaller, systems. In the present study, the Fermi-contact components of the J values were computed directly via DFT, presumably recovering the important effects of electron correlation and thus obviating the need for scaling. J_{CH} values (one-, two-, and three-bond) derived from the DFT treatment are compared to scaled couplings obtained previously using HF/MP2 methods. The effect of structural relaxation on J is assessed by direct comparison of HF values for the $^{13}C-^{1}H$ couplings in both HF- and DFT-optimized geometries. $^{1}J_{CC}$, $^{2}J_{CC}$, $^{3}J_{CC}$, and $^{2+3}J_{CC}$ values are computed (DFT) in **1** as a function of ring conformation for the first time, correlation corrections are evaluated by direct comparison with HF calculations, and new structural interpretations of these couplings are provided.

Introduction

Conformational analysis of biomolecules by NMR spectroscopy depends, in part, on the accurate measurement and interpretation of scalar spin−spin coupling constants (J couplings), especially those across three bonds (vicinal couplings, ^{3}J). The latter values depend, among other factors, on the dihedral angle between the coupled atoms, as first described by Karplus,[1] and numerous studies have defined correlations between molecular structure and ^{3}J values in a wide range of compounds.[2] In contrast, one-bond (^{1}J) and two-bond (^{2}J) couplings are applied less often in conformational analysis partly because their dependencies on molecular structure are not as well appreciated or understood, although some notable exceptions exist.[3−12] Vicinal spin couplings between protons ($^{3}J_{HH}$) are most commonly applied in structural studies due to their relative ease of measurement and the wealth of information correlating their magnitudes with molecular structure.[13] However, with the development of modern NMR techniques,[14,15] accurate spin coupling constants can be measured involving other nuclei such as carbon. Since J_{CH} and J_{CC} values are frequently more abundant in molecules than $^{3}J_{HH}$ values, these couplings represent a potentially valuable source of structural information.

The analysis of J couplings in structure determinations is most valuable in molecules that are conformationally flexible. In these cases, the presence of populations of different, interconverting molecules in solution gives rise to averaged NMR parameters, and this averaging is not always linear, as discussed by Jardetzky.[16] For example, $^{1}H-^{1}H$ nuclear Overhauser effects (NOEs) depend on the distance, r, between proton pairs as r^{-6}, and thus the observed NOEs in flexible systems will be highly skewed in favor of conformers containing the smaller internuclear distances.[17] This latter effect introduces complications in the structural interpretation of NOE values, especially when only a small number can be observed. On the other hand, scalar couplings are averaged linearly, and thus their interpretation in the presence of conformational flexibility is, in principle, less prone to error.

Recently we applied experimental and theoretical methods to evaluate the behavior of J_{CH} values in biologically relevant β-D-ribofuranosyl and 2-deoxy-β-D-*erythro*-pentofuranosyl rings.[18,19] Ab initio self-consistent field (SCF) molecular orbital calculations using a split-valence basis set (6-31G*) gave optimized structures for the 10 nonplanar (envelope) forms of these rings, and $^{1}J_{CH}$, $^{2}J_{CH}$, and $^{3}J_{CH}$ values were computed in each conformer. $^{n}J_{CH}$ values were first computed at the HF level using finite-field perturbation theory and a previously introduced basis set[20] designed to economically recover the Fermi-contact contribution to $^{13}C-^{13}C$ spin−spin coupling constants. Electron correlation effects on the coupling constants were then introduced via second-order Møller−Plesset perturbation (MP2) calculations with the same basis set. The derived correlation corrections (i.e., MP2 − HF values) were scaled by factors

* Authors for correspondence.
[†] Department of Chemistry and Biochemistry.
[‡] Radiation Laboratory.

10.1021/jp9905676 CCC: $18.00
Published on Web 04/29/1999

obtained from more elaborate quadratic configuration interaction (QCISD) calculations on related systems.[21] These scaled coupling constants were combined with experimental measurements to establish the dependencies of J_{CH} values on furanosyl ring conformation and on carbohydrate structure in general. However, while this theoretical approach predicts reliable coupling *trends*, it suffered from some limitations. First, geometrical parameters were determined at the HF level of theory, and thus electron correlation effects on structural optimization were neglected. While correlation corrections were included in the spin coupling calculations, they were overestimated at MP2. Furthermore, the required scaling factors depend on the nature and separation of the coupled nuclei, the chemical bonding along the coupling path, and the basis set employed in the calculation. Reliable evaluation of these scaling factors thus required extensive comparison with results from more accurate treatments of electron correlation (QCISD) in a wide range of related model compounds whose sizes were kept relatively small in order to ensure practicable computations.

These limitations prompted us to examine the use of density functional theory (DFT) in such studies, since DFT methods are intended to economically recover the important effects of electron correlation. For example, Bauschlicher[22] has shown the considerable improvements, compared to HF results, in the determination of structural parameters, particularly when hybrid functionals are used. Malkin et al.[23a] have shown that DFT methods yield reliable NMR chemical shifts and spin−spin coupling constants, at least in small hydrocarbons, Stahl et al.[23b] have shown that reliable J_{CC} values could be calculated by DFT in an acyclic alkene, and a recent study of methyl β-D-xylopyranoside by Hricovini et al.[23c] has demonstrated the usefulness of DFT in predicting ^{1}H, ^{13}C, and ^{17}O chemical shifts and J_{CH} values, in carbohydrates. Further validation of the DFT approach as applied to carbohydrate systems thus appeared attractive in order to identify potential advantages and limitations prior to its application in more complex carbohydrate-containing systems.

In this investigation, the DFT method has been applied to predict molecular parameters (bond lengths, bond angles, bond torsions) in the 10 geometrically optimized envelope forms of 2-deoxy-β-D-*erythro*-pentofuranose (**1**). These structural parameters are compared to those reported previously at the HF/6-31G* level of theory.[19] J_{CH} values (one-, two-, and three-bond) in **1** are then computed using the DFT-optimized geometries and are compared to the scaled couplings reported previously using HF and MP2 methods[19] and scaling procedures described above. Finally, $^{1}J_{CC}$, $^{2}J_{CC}$, $^{3}J_{CC}$, and $^{2+3}J_{CC}$ values are computed in **1** for the first time, and structural interpretations of these couplings are provided. These calculations were performed with DFT-optimized geometries using both HF and DFT approaches, thus allowing a direct comparison of the improvements afforded by the latter treatment.

Computational Methods

All calculations were performed with a modified[20] version of the Gaussian 94 suite of programs.[24] Electron correlation effects were treated by means of DFT. The standard B3LYP functional, due to Becke,[25] was used throughout. This functional comprises both local[26] and nonlocal[27] exchange contributions and contains terms accounting for local[28] and nonlocal[29] correlation corrections. The B3LYP functional was chosen on two grounds. First, DFT with this functional has been shown to produce structural parameters in close accord with experiment.[22] Second, functionals such as B3LYP, which include a piece of true HF exchange, have been shown[30] to provide a particularly reliable description of the unpaired spin distribution in radicals.

Geometry Optimization. Geometries were optimized in constrained envelope forms (one endocyclic torsion angle was held constant at 0°) as before[19] using the B3LYP functional and the standard 6-31G* basis set. Initial values for the exocyclic torsions were chosen as before:[19] (a) the C1−O1 torsion was chosen to maximize the exoanomeric effect[31−33] (OH-1 *anti* to C2); (b) OH-3 *anti* to C4; (c) C4−C5 in the *gt* conformation (O5 *anti* to C3); (d) OH-5 *anti* to C4.

Calculation of *J* Couplings. All indirect spin−spin coupling constants in the optimized structures were determined using a previously constructed basis set[20] by finite (Fermi-contact)-field double perturbation theory.[34] Suitable values for the perturbing fields for the various couplings were chosen to ensure sufficient numerical precision while still allowing a satisfactory low-order finite-difference representation of the effect of the perturbation. As before, only the Fermi-contact component of each coupling constant was recovered.

Results and Discussion

Optimized Structural Parameters and Conformational Energies. In a prior investigation,[19] a detailed analysis of conformational energies, structural parameters, and computed J_{CH} values in **1** was reported using HF methods, and experimental couplings in methyl 2-deoxy-β-D-*erythro*-pentofuranoside (**2**) were examined in light of the computed behavior. The aim of the following discussion is to compare conformational energies and optimized structural parameters in **1** derived from the HF (prior results) and DFT (present study) methodologies.

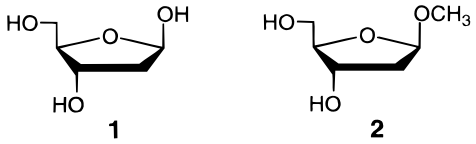

Conformational energies for **1** computed using the HF and DFT methods are shown in Figure 1A. The overall shape of the conformational energy curve is conserved in the two treatments; the global energy minimum is located at E_2 and a local minimum at ^{4}E, the latter being better defined in the HF treatment. Virtually identical relative energies are obtained for 7 of the 10 envelope forms; in ^{4}E, E_o, and ^{1}E, significant differences are observed, with the DFT treatment yielding smaller relative energies. Electron correlation effects are apparently more significant in these western conformers of **1**. The amplitudes of the two curves are similar, with an energy difference of ∼3.3 kcal/mol predicted between the most (E_2) and least (E_1) stable conformers.

Bond lengths (C−H, C−O, and C−C) calculated by the DFT method are 0.4−1.9% larger than corresponding bond lengths calculated by the HF method (Figure 1B−D; see Supporting Information). Thus, the DFT method produces more relaxed structures than the HF treatment, in agreement with results from more traditional electron correlation techniques.[35] However, both methods predict the same *dependencies* of bond length on ring conformation, which have been discussed in earlier reports.[18,19,36−38] It should be noted, for example, that the C1−O1, C1−O4, and C1−H1 bond lengths display the expected dependencies on ring conformation. The exocyclic bonds (C1−O1, C1−H1) are shortest when quasi-equatorial or near-quasi-equatorial (e.g., ^{o}E/E_1 for C1−O1; E_o/^{1}E for C1−H1) and longest when quasi-axial or near-quasi-axial (e.g., E_o/

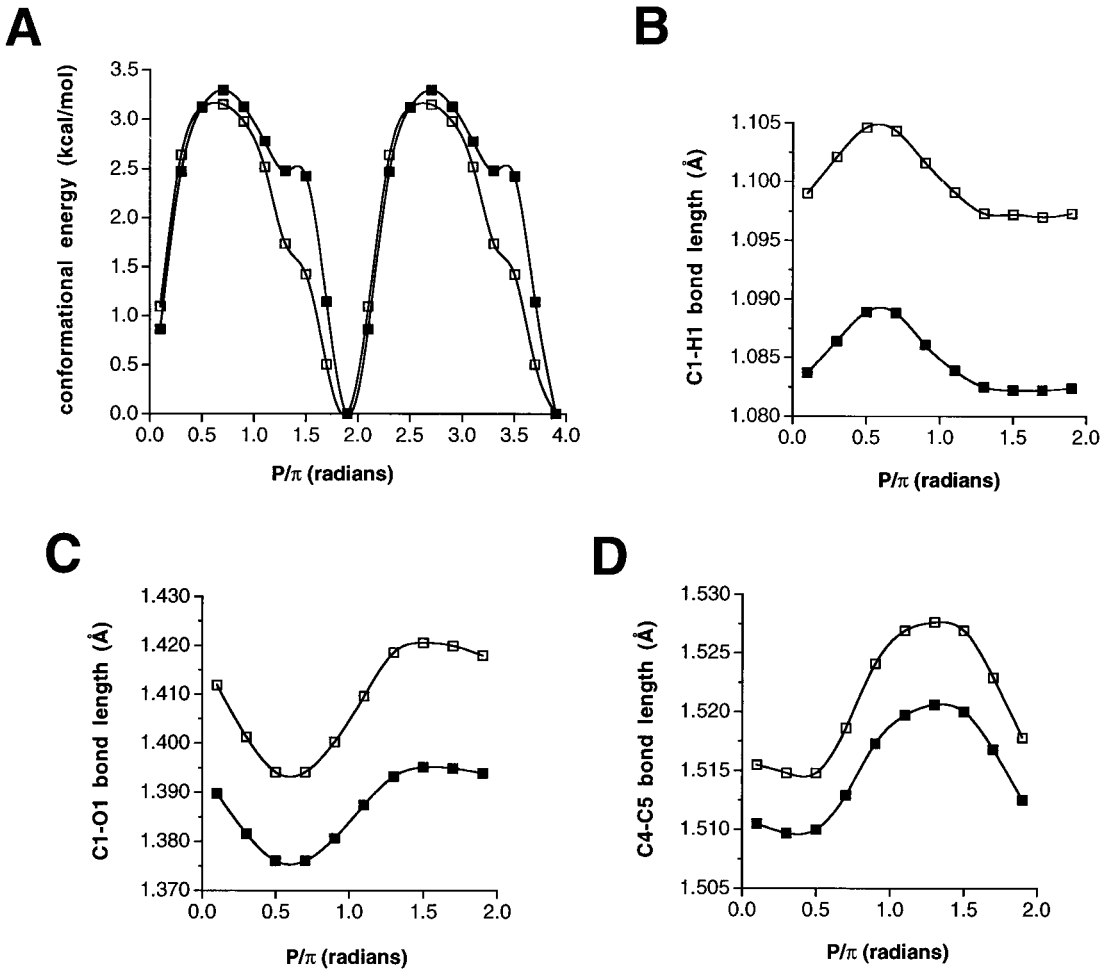

Figure 1. Effect of ring conformation on (A) conformational energy profiles, (B) C1−H1 bond length, (C) C1−O1 bond length, and (D) C4−C5 bond length for **1** obtained from ab initio molecular orbital calculations using the HF (■) and DFT (□) methods and the 6-31G* basis set.

^{1}E for C1−O1; ^{o}E/E$_1$ for C1−H1). The behavior of the C1−O4 bond length is explained by noting that it is maximal near ^{o}E/E$_1$ and minimal near E$_o$. Maximal $n \rightarrow \sigma^*$ donation by the ring oxygen is expected when the C1−O1 bond is axial, that is, in E$_o$/^{1}E conformations.[39] In these geometries, the C1−O1 bond should lengthen and the C1−O4 bond should contract due to the anomeric effect in furanoses,[40,41] in agreement with the computed behavior.

Other key molecular parameters such as C1−O1 and C3−O3 torsion angles, puckering amplitude (τ_m), and C1−O4−C4 bond angle show similar overall dependencies on ring conformation in both treatments (data not shown; see Supporting Information). The C1−O1 torsion experiences greater amplitude in the DFT treatment; this torsion is influenced by stereoelectronic factors (exoanomeric effect[31−33]), and its behavior may thus be more affected than other C−O torsions (e.g., the C3−O3 torsion where the HF and DFT curves are more similar) when electron correlation effects are included in the calculations. Puckering behavior is very similar in the DFT and HF treatments, and a slightly smaller C1−O4−C4 bond angle (by ∼1°) is calculated for all ring conformations using the DFT method.

These results show that similar trends in optimized structural parameters in the 10 envelope conformers of **1** are predicted by the HF and DFT methods. The HF approach is known to produce bond lengths which are markedly too short, at least for flexible basis sets, so that the DFT predictions, which are systematically longer here, are presumably in closer accord with experiment.

Spin Coupling Constants. *1. $^{13}C-^1H$ Spin Coupling Constants.* Figure 2A,C−F presents a comparison between the previously reported scaled (HF/MP2) couplings and the present DFT-derived values. These coupling constants were, of course, obtained using different optimized geometries. C−H bonds are noticeably longer in DFT-optimized structures, and the effect of this relaxation on J_{CH} was determined by comparing *unscaled* HF/[5s2p1d,2s] calculations of $^1J_{C1,H1}$ using HF- and DFT-optimized geometries (Figure 2B). The longer bonds in the DFT geometries gave *larger* unscaled HF values of $^1J_{C1,H1}$ and for the remaining $^1J_{CH}$ in **1** (data not shown), with differences ranging from 3.3 Hz for $^1J_{C2,H2R}$ to 9.2 Hz for $^1J_{C1,H1}$ (values averaged over the pseudorotational itinerary). These data suggest that geometry optimization using DFT makes a substantial contribution to the differences observed between the scaled couplings and the DFT-derived $^1J_{CH}$ values. However, the larger unscaled HF $^1J_{CH}$ values obtained using DFT geometries may yield *scaled* $^1J_{CH}$ values in better agreement with experiment than *scaled* HF values using HF geometries, although this test was not conducted. In contrast, HF/[5s2p1d,2s] calculations of $^2J_{CH}$ in **1** showed only small (<0.6 Hz) shifts to more negative values on moving to the DFT structures, and $^3J_{CH}$ values were essentially unchanged (data not shown).

Computed $^1J_{CH}$ values in **1** are consistently larger in DFT calculations than the corresponding scaled (HF/MP2) values; however, coupling *trends* predicted by both methods are virtually identical. Thus, for example, computed $^1J_{C1,H1}$ values range from 152 to 161 Hz in the (scaled) HF treatment and from 161 to 171 Hz in the DFT analysis, translating into a ∼6% increase in

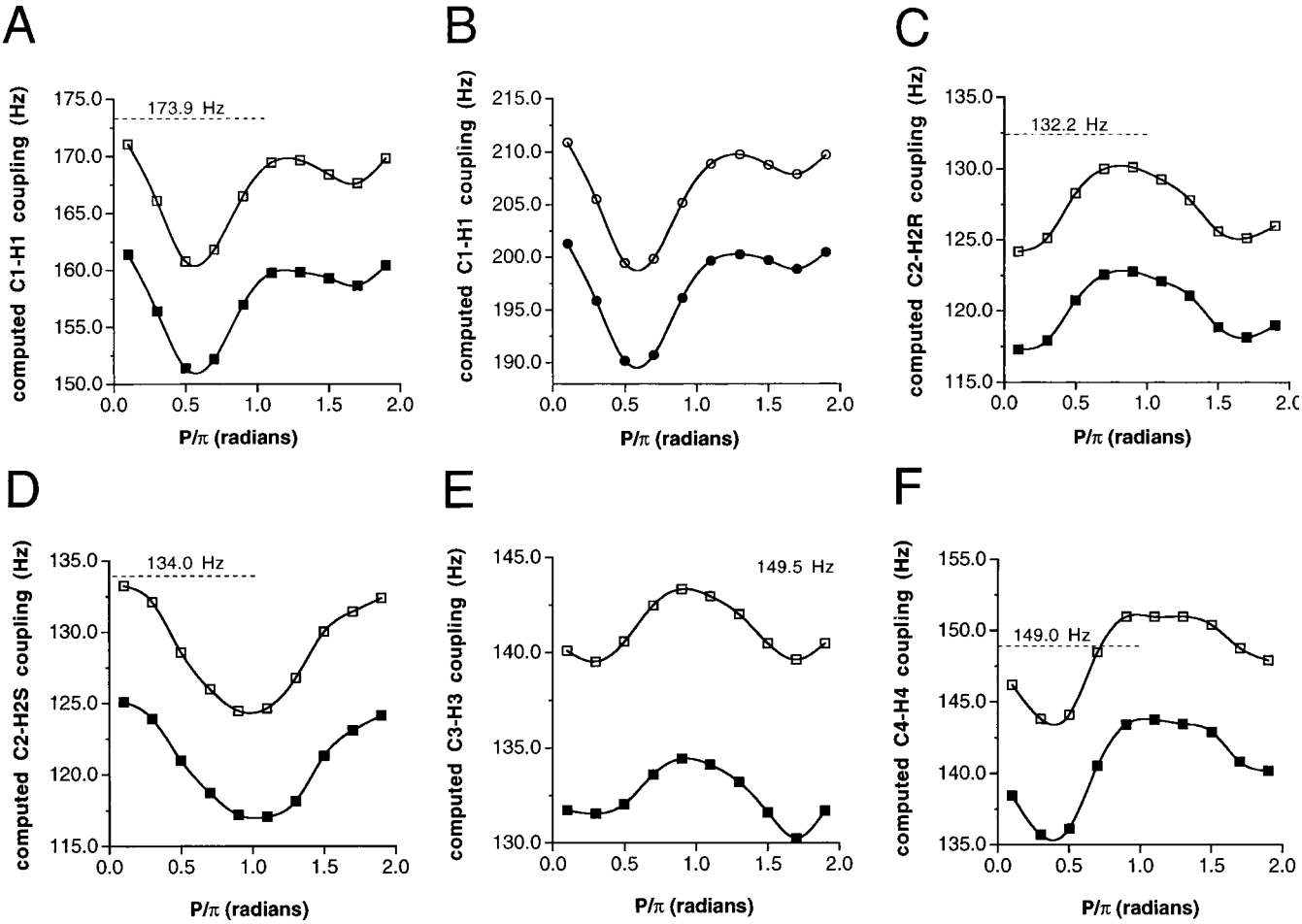

Figure 2. Computed $^1J_{CH}$ values in **1** as a function of ring conformation—scaled values at HF/6-31G* geometries (■) and DFT values at B3LYP/6-31G* geometries (□): (A) $^1J_{C1,H1}$; (B) $^1J_{C1,H1}$, unscaled HF values (●) and unscaled HF values using DFT-optimized geometries (○); (C) $^1J_{C2,H2R}$; (D) $^1J_{C2,H2S}$; (E) $^1J_{C3,H3}$; (F) $^1J_{C4,H4}$. Dotted lines and accompanying values are the corresponding experimental $^1J_{CH}$ values observed in **2**.

coupling magnitude (Figure 2A). Similar percent increases are observed for $^1J_{C2,H2R}$ (∼6%), $^1J_{C2,H2S}$ (∼7%), $^1J_{C3,H3}$ (∼7%), and $^1J_{C4,H4}$ (∼5%). Much of these increases are correlated with C−H bond lengthening between the HF and DFT treatments; however, small residual discrepancies of up to 3.5 Hz (for $^1J_{C2,H2R}$) remain even after this is taken into consideration. Importantly, the DFT-derived couplings are in closer agreement with experimental couplings than scaled values obtained at HF geometries ($^1J_{CH}$ values in aldopyranosyl and aldofuranosyl rings typically range from ∼160 to ∼175 Hz), suggesting that the inclusion of electron correlation by the DFT method improves the accuracy of computed J_{CH} values. For example, $^1J_{C1,H1}$ = 173.9 Hz in methyl 2-deoxy-β-D-*erythro*-pentofuranoside (**2**), a value which deviates significantly from the range of couplings computed by HF methods. The observed range of $^1J_{CH}$ values from DFT analysis still does not include the observed value, but the agreement is improved and the residual deviation may be due in part to limiting the computations to a single combination of exocyclic torsions in **1**, solvent effects, and/or effects of methyl glycosidation on $^1J_{C1,H1}$ values, in addition to the more technical factors of basis set limitations and the choice of functional.

Two-bond $^{13}C-^1H$ couplings determined by the DFT method are consistently *more positive* than HF-derived values (Figure 3). Thus, for example, $^2J_{C1,H2R}$ and $^2J_{C3,H2S}$ are shifted by ∼+1 Hz in all ring conformations, whereas smaller differences are observed for $^2J_{C1,H2S}$, $^2J_{C2,H1}$, $^2J_{C2,H3}$, $^2J_{C3,H2R}$, $^2J_{C3,H4}$, and $^2J_{C4,H3}$. As observed for $^1J_{CH}$ values, the coupling trends predicted by the HF treatment are reproduced by the DFT analysis. As mentioned above, HF calculations (unscaled) at the DFT geometries showed small negative shifts from values obtained in HF-optimized structures.

The high level of agreement between computed $^2J_{CH}$ values in **1** and experimentally observed couplings in **2** is encouraging. For example, experimentally observed values of $^2J_{C1,H2R}$, $^2J_{C1,H2S}$, $^2J_{C2,H3}$, $^2J_{C3,H2R}$, $^2J_{C3,H2S}$, and $^2J_{C4,H3}$ in **2** fall within the range of computed values, and excellent agreement is observed with respect to coupling signs. Computed $^2J_{CH}$ values probably contain the same errors as $^1J_{CH}$ values (up to ∼10%), but this translates into a much smaller absolute error (<1 Hz) for the two-bond couplings. Observed $^2J_{C2,H1}$ and $^2J_{C3,H4}$ values fall outside the range predicted by the computations, and these deviations may reflect the effects of methyl glycosidation (for $^2J_{C2,H1}$) and hydroxymethyl rotation (for $^2J_{C3,H4}$) on these couplings (i.e., significant structural differences between **1** in vacuo and **2** in solution prevent the direct comparison of the calculated and observed couplings).

The computed $^2J_{CH}$ values involving the hydroxymethyl protons ($^2J_{C4,H5R}$ and $^2J_{C4,H5S}$) behave as predicted recently[19,42,43] (via the projection rule[5a]) for the *gt* rotamer (Figure 4A,B). In this rotamer, the former is negative in sign, whereas the latter is positive. However, it should be appreciated that the Perlin[5b] and Pedersen[5a] empirical methods predict either *small* negative or *large* positive couplings for $^2J_{C4,H5R}$ and $^2J_{C4,H5S}$, respectively, in the *gt* rotamer. By comparison, the computations predict a −5.6 to −6.0 range for $^2J_{C4,H5R}$ and +0.3 to +1.6 Hz range for $^2J_{C4,H5S}$. Griesinger and co-workers reported $^2J_{C4,H5R}$ values of −1.5 to +1.4 Hz and $^2J_{C4,H5S}$ values of −3.0 to −6.7 Hz in

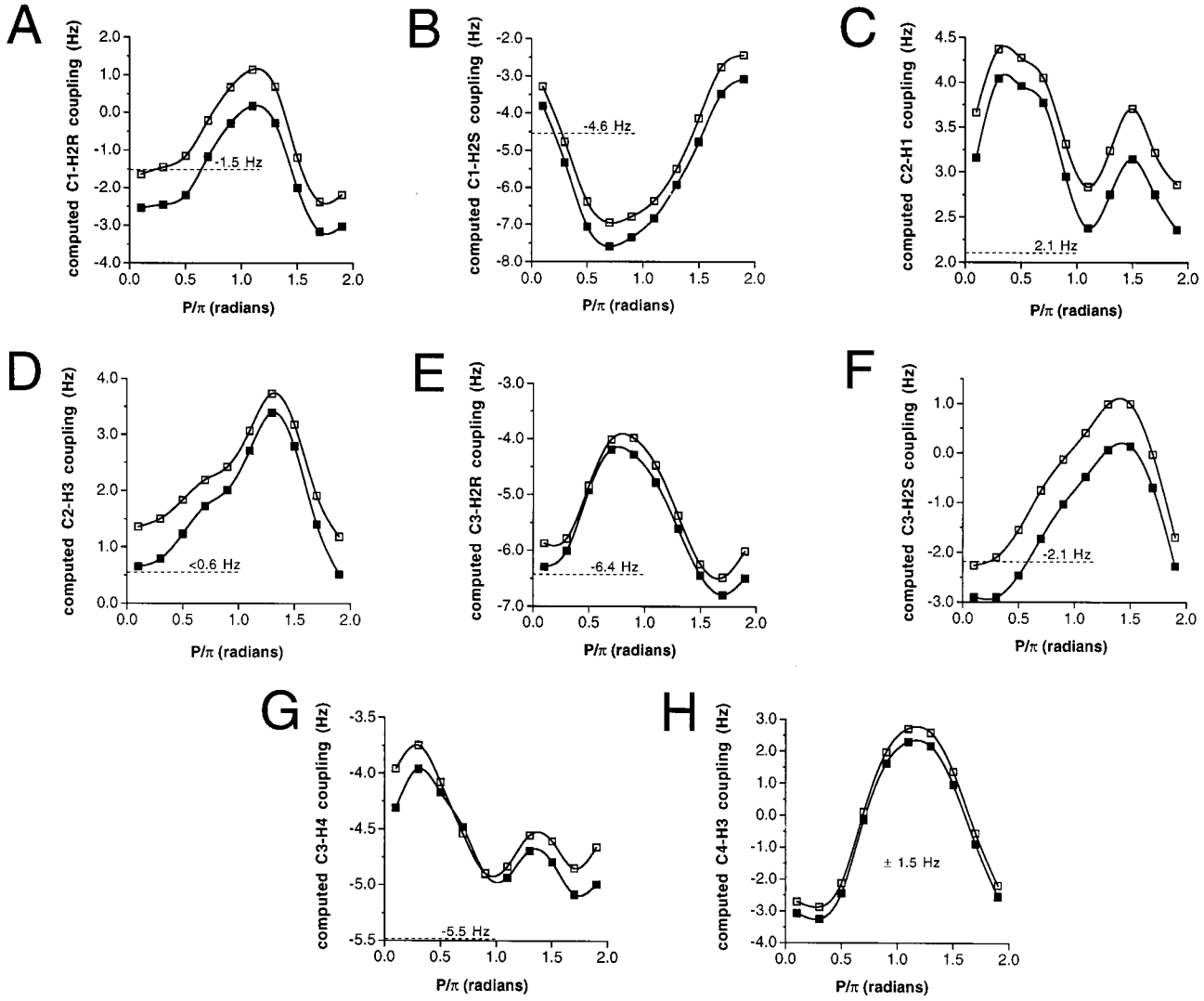

Figure 3. Computed endocyclic $^2J_{CH}$ values in **1** as a function of ring conformation—scaled values at HF/6-31G* geometries (■) and DFT values at B3LYP/6-31G* geometries (□): (A) $^2J_{C1,H2R}$; (B) $^2J_{C1,H2S}$; (C) $^2J_{C2,H1}$; (D) $^2J_{C2,H3}$; (E) $^2J_{C3,H2R}$; (F) $^2J_{C3,H2S}$; (G) $^2J_{C3,H4}$; (H) $^2J_{C4,H3}$. Dotted lines and accompanying values are the corresponding experimental $^2J_{CH}$ values observed in **2**.

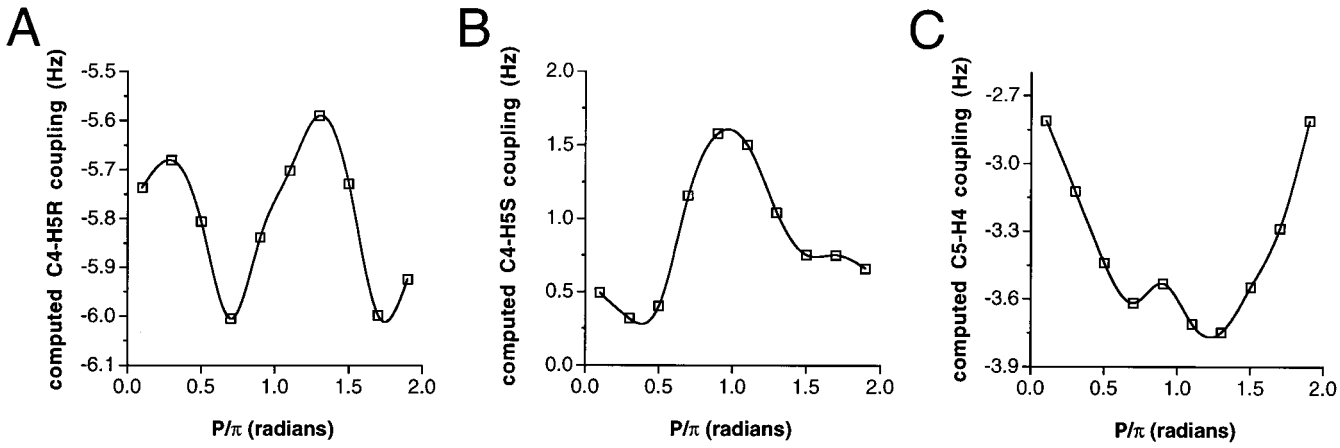

Figure 4. Computed exocyclic $^2J_{CH}$ values in **1** as a function of ring conformation determined by the DFT method ([5s2p1d|2s] basis set) at B3LYP/6-31G* geometries: (A) $^2J_{C4,H5R}$; (B) $^2J_{C4,H5S}$; (C) $^2J_{C5,H4}$.

RNA oligomers where the *gg* conformer is favored;[43] their prediction of coupling *magnitudes* in this rotamer also contradicts predictions based on the Perlin and Pedersen rules. The disparity is most likely due to the fact that the Perlin rules are based on couplings in (HO)C−C or $(OH)_2$C−C fragments and the Pederson projection curve was developed for $(HO)_2$C−C(OH) fragments, which differ from the (HO)C−C(OH) fragment relevant for $^2J_{C4,H5R/S}$ analysis. An examination of $^2J_{CH}$ values in conformationally rigid aldohexopyranosyl rings[44] containing (HO)C−C(OH) pathways (e.g., $^2J_{C2,H3}$, $^2J_{C3,H2}$, $^2J_{C3,H4}$) shows that a projection of 0 corresponds to a coupling of −4.8 ± 0.7 Hz (13 compounds) and a projection of 1.5

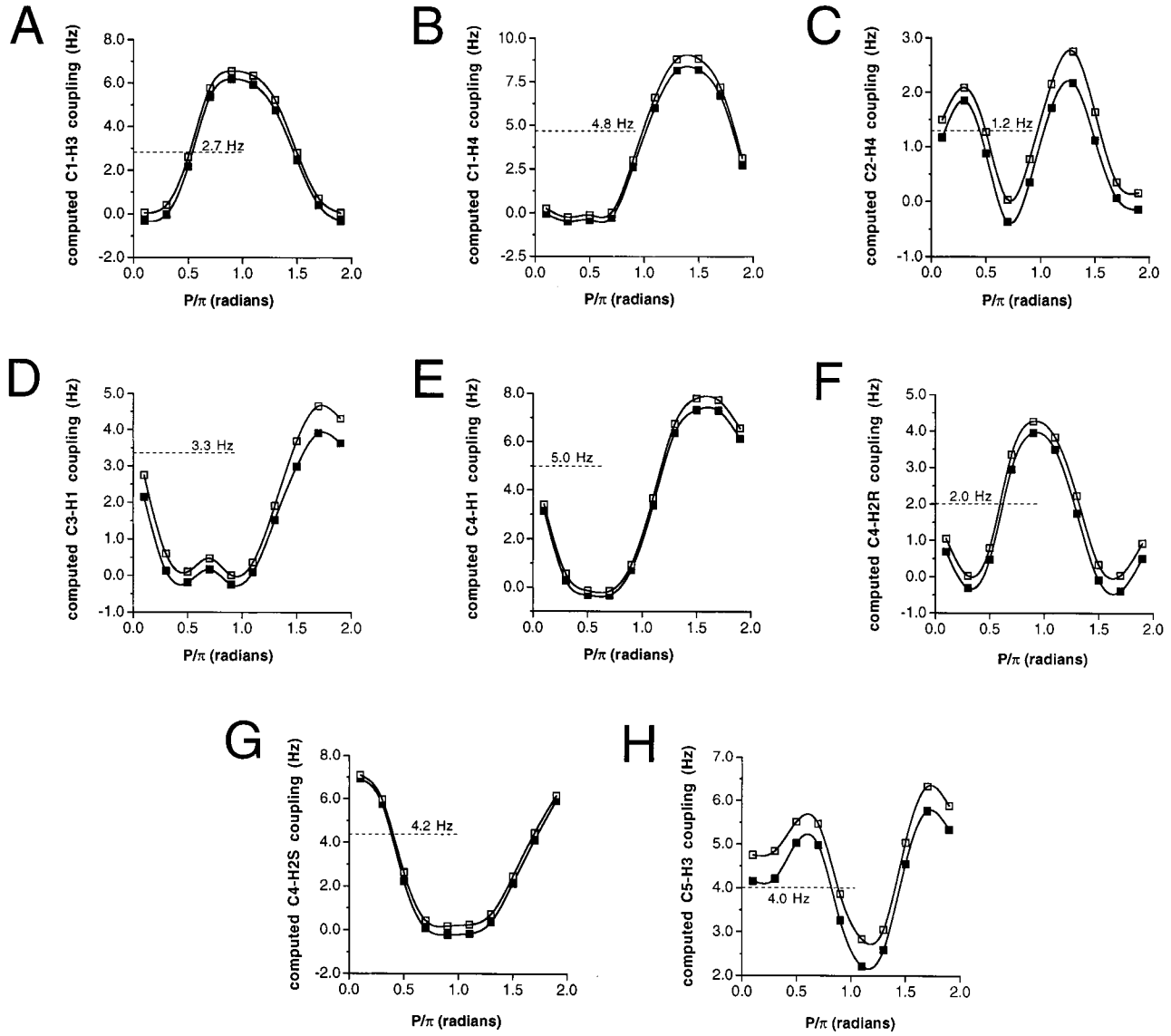

Figure 5. Computed $^3J_{CH}$ values in **1** as a function of ring conformation—scaled values at HF/6-31G* geometries (■) and DFT values at B3LYP/6-31G* geometries (□): (A) $^3J_{C1,H3}$; (B) $^3J_{C1,H4}$; (C) $^3J_{C2,H4}$; (D) $^3J_{C3,H1}$; (E) $^3J_{C4,H1}$; (F) $^3J_{C4,H2R}$; (G) $^3J_{C4,H2S}$; (H) $^3J_{C5,H3}$. Dotted lines and accompanying values are the corresponding experimental $^3J_{CH}$ values observed in **2**.

corresponds to a coupling of 1.4 ± 0.5 Hz (5 compounds). These results are more consistent with the computed behavior of $^2J_{C4,H5R}$ and $^2J_{C4,H5S}$ in **1** (we assume here that the behavior of $^2J_{CH}$ values in (HO)C−C(OH) pathways is not affected significantly by whether one of the carbons in the coupling fragment is a terminal carbon) with respect to magnitude and sign and suggest that a modified projection curve may apply to (HO)C−C(OH) pathways, as implied by Bock and Pedersen in the original description of their method.[5a]

$^2J_{C5,H4}$ was predicted earlier to be small and negative for the *gt* conformer in **1** using the projection rule,[5a] and the sign prediction is confirmed by the computed data (Figure 4C). The computed coupling magnitudes, however, are somewhat more negative than predicted by the Perlin and Pedersen rules, apparently for the same reasons discussed above for $^2J_{C4,H5R/S}$.

Three-bond $^{13}C-^1H$ spin couplings are virtually identical in magnitude in the scaled HF and DFT treatments (Figure 5). When differences can be discerned, the DFT calculations produce slightly larger couplings (<0.5 Hz difference). As observed for $^1J_{CH}$ and $^2J_{CH}$, virtually identical dependencies of $^3J_{CH}$ on ring conformation are obtained by the HF and DFT treatments. Again, as mentioned above, there is little change in the HF/[5s2p1d,2s] computed $^3J_{CH}$ values on moving between the HF- and DFT-optimized structures (data not shown). This is in accord with the insensitivity to optimization method of the dihedral angle separating the coupled nuclei.

The observed $^3J_{CH}$ values in **2** involving ring protons lie in the range of the computed couplings in all cases (Figure 5). Thus, for example, $^3J_{C1,H3} = 2.7$ Hz in **2**, and the computed couplings range from ∼0 to 6.5 Hz. The agreement between experimental and computed couplings suggests that the DFT and scaled HF methods are nearly quantitative, which contrasts with observations made for $^1J_{CH}$ and $^2J_{CH}$ values, where differences in experimental and computed couplings were observed (i.e., experimental couplings fell outside of the predicted ranges in some cases). The better agreement suggests that $^3J_{CH}$ values may be less sensitive to exocyclic C−C and C−O torsions than $^1J_{CH}$ and $^2J_{CH}$ values.

The exocyclic C3−C4−C5−H5*R*/*S* torsion angles in the *gt* rotamer of **1** vary slightly with ring conformation, as shown in Figure 6A,B. The approximately *gauche* dihedral angles yield small values for $^3J_{C3,H5R}$ and $^3J_{C3,H5S}$ (0.5−1.5 Hz) (Figure 6C). The small dependence of these couplings on ring conformation, however, cannot be directly correlated with changes in C−C−

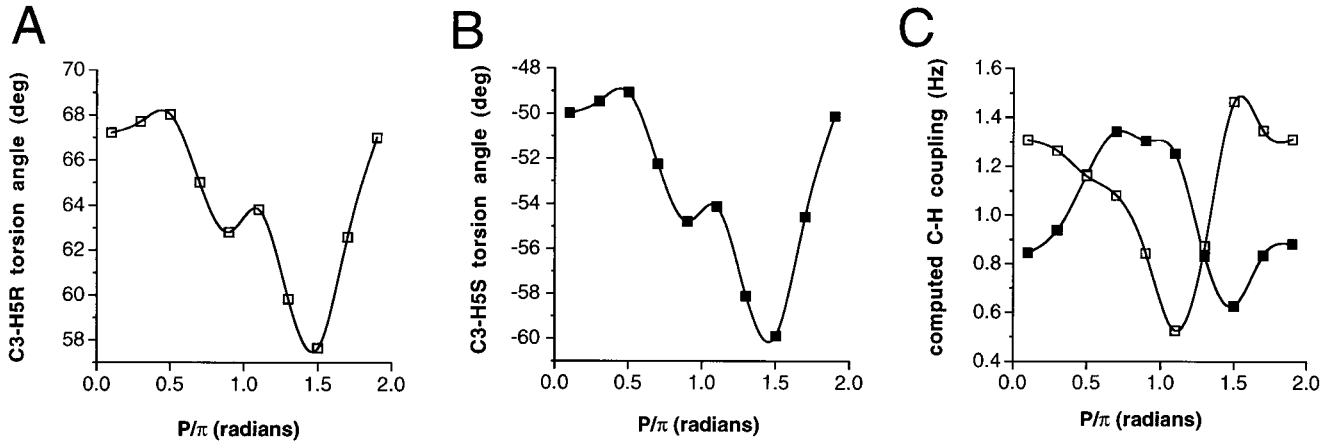

Figure 6. Exocyclic C3−H5*R* (A) and C3−H5*S* (B) torsion angles in **1** as a function of ring conformation (B3LYP/6-31G*) and the corresponding couplings (C) determined by the DFT method ([5s2p1d|2s] basis set) at B3LYP/6-31G* geometries ($^3J_{C3,H5R}$, □; $^3J_{C3,H5S}$, ■).

C−H dihedral angles, suggesting that other unidentified factors influence their magnitudes.

A total of 10 $^3J_{CH}$ values were calculated in **1**, namely, $^3J_{C1,H3}$, $^3J_{C1,H4}$, $^3J_{C2,H4}$, $^3J_{C3,H1}$, $^3J_{C3,H5R}$, $^3J_{C3,H5S}$, $^3J_{C4,H1}$, $^3J_{C4,H2R}$, $^3J_{C4,H2S}$, and $^3J_{C5,H3}$. Correlations between these couplings and dihedral angle (for plots of C−H dihedral angles as a function of ring conformation, see Supporting Information) are shown in Figure 7. The composite curve (Figure 7A) is consistent with expectation, with minimal coupling observed at $\Theta = \sim 90°$ and maximal coupling observed at $\Theta = 0°$ and 180°. Two of the 10 available $^3J_{CH}$ values involve C−O−C−H coupling pathways ($^3J_{C1,H4}$, $^3J_{C4,H1}$), while the remainder involve C−C−C−H pathways. The latter can be divided into three distinct types, namely, (OH)-*C*CC(OH)*H*, (OR)CCC*H*, and *C*CC(OR)*H*, where the italicized nuclei are coupled and the intervening carbons in the pathway have one oxygen substituent. Karplus behaviors of these four different pathways are not expected to be identical, which leads to significant scatter in the composite curve (Figure 7A). Individual Karplus curves (Figure 7B−D) exhibit less scatter and reveal subtle differences between the pathways. The C−O−C−H pathway (Figure 7C) exhibits the greatest amplitude, as expected; previous results in aldopyranosyl rings show that substitution of an oxygen atom for carbon in a C−C−C−H coupling pathway enhances coupling.[44] These results are in fair agreement with Karplus relationships derived experimentally using conformationally fixed model compounds.[45−48]

2. $^{13}C-^{13}C$ Spin Coupling Constants. A. One-Bond Couplings. $^1J_{C1,C2}$ is relatively constant throughout the pseudorotational itinerary, varying from 41 to 42.5 Hz, with the minimal coupling observed at E_4 (Figure 8A). In contrast, $^1J_{C2,C3}$ exhibits considerable change with ring conformation, varying from 35.4 Hz (E_3) to 39.9 Hz (^oE) (Figure 8C). $^1J_{C3,C4}$ varies slightly with ring conformation, with a minimal value (39.2 Hz) observed at E_1 and a maximal value (42.7 Hz) observed at ^1E (Figure 8E). The exocyclic $^1J_{C4,C5}$ varies significantly with ring conformation; minimal coupling (44.0 Hz) is observed at ^4E, and maximal coupling (48.4 Hz) is observed at ^oE (Figure 8G). The computed relative magnitudes of $^1J_{CC}$ values in **1** are in reasonable agreement with relative magnitudes observed experimentally in **2**, where $^1J_{C4,C5} > {}^1J_{C1,C2} > {}^1J_{C3,C4} > {}^1J_{C2,C3}$. In contrast to $^1J_{CH}$ values, $^1J_{CC}$ values computed by the DFT method are *larger* than experimental couplings, and it is interesting to note that the approximate percent increase in the computed $^1J_{CC}$ values with respect to the experimental values is not constant: $^1J_{C1,C2}$, ∼3%; $^1J_{C2,C3}$, ∼5%; $^1J_{C3,C4}$, ∼9%; $^1J_{C4,C5}$, ∼12%. We attribute the larger percent difference in $^1J_{C3,C4}$ to our initial choice of C3−O3 torsion angle (OH-3 approximately *anti* to C4) which yields a maximal value for this interaction. $^1J_{C4,C5}$ depends on hydroxymethyl conformation, which differs in the in vacuo calculations and in solution; the computed couplings pertain to only one C4−C5 rotamer (*gt*), whereas in solution all three rotamers are populated, albeit to different extents.[19] As described earlier, $^1J_{CC}$ values for vicinal diol fragments depend on the C−C torsion angle.[49] Differences in the C5−O5 torsional behavior between the computational model and molecules in solution are also expected to affect $^1J_{C4,C5}$ magnitude.[49] As observed for other exocyclic substituents, the C4−C5 bond varies with orientation (quasi-axial, ^4E, longer; quasi-equatorial, E_4, shorter) (Figure 1D), and this dependence affects $^1J_{C4,C5}$ magnitude in a predictable manner (longer bond, less *s*-character, smaller *J*; shorter bond, more *s*-character, larger *J*) (Figure 8G).

Endocyclic C−C bond lengths vary with ring conformation in **1** in a predictable fashion (data not shown; see Supporting Information). Previous studies of C−C behavior in furanosyl rings have shown that a given C−C bond is lengthened when the ring atom opposite to it is out-of-plane and reduced when both carbons in the C−C bond are out-of-plane. Thus, the C1−C2 bond length is maximal when C4 is out-of-plane (P/π = 0.3 and 1.3) and minimal in the $^2T_1$ and $^1T_2$ conformers. The C2−C3 bond length is maximal when O4 is out-of-plane (P/π = 0.5 and 1.5) and minimal in the $^2T_3$ and $^3T_2$ conformers. The C3−C4 bond length is maximal when C1 is out-of-plane (P/π = 0.7 and 1.7) and minimal in the $^3T_4$ and $^4T_3$ conformers. Thus, on the basis of bond length considerations alone, endocyclic $^1J_{CC}$ values might be expected to vary with ring conformation, with shorter bonds yielding larger couplings, but this prediction is not supported by the computations. For example, for $^1J_{C2,C3}$, comparable coupling minima are observed in the $^2T_3$ and $^3T_2$ conformers where bond length is *minimal*, and different coupling maxima are found at ^oE and $\sim E_o$ where bond length is *maximal*. Clearly, factors other than, or in addition to, bond length determine the dependence of *endocyclic* $^1J_{CC}$ values on ring conformation.

B. Two-Bond Couplings. Only one $^2J_{CC}$ value exists in **1**, namely, $^2J_{C3,C5}$, and predictions of its magnitude and sign have been made previously.[50,51] This coupling will be affected by the relative disposition of the terminal electronegative substituents, O3 and O5, with an in-plane orientation (O3−C3−C4−C5−O5 coplanar) producing the largest (most positive) coupling. The relative orientation of the terminal OH substituents depends on ring conformation, with the in-plane orientation attained in conformations near $E_3/^4E$ (P/π = 1.1 and 1.3) (*gt* rotamer). The

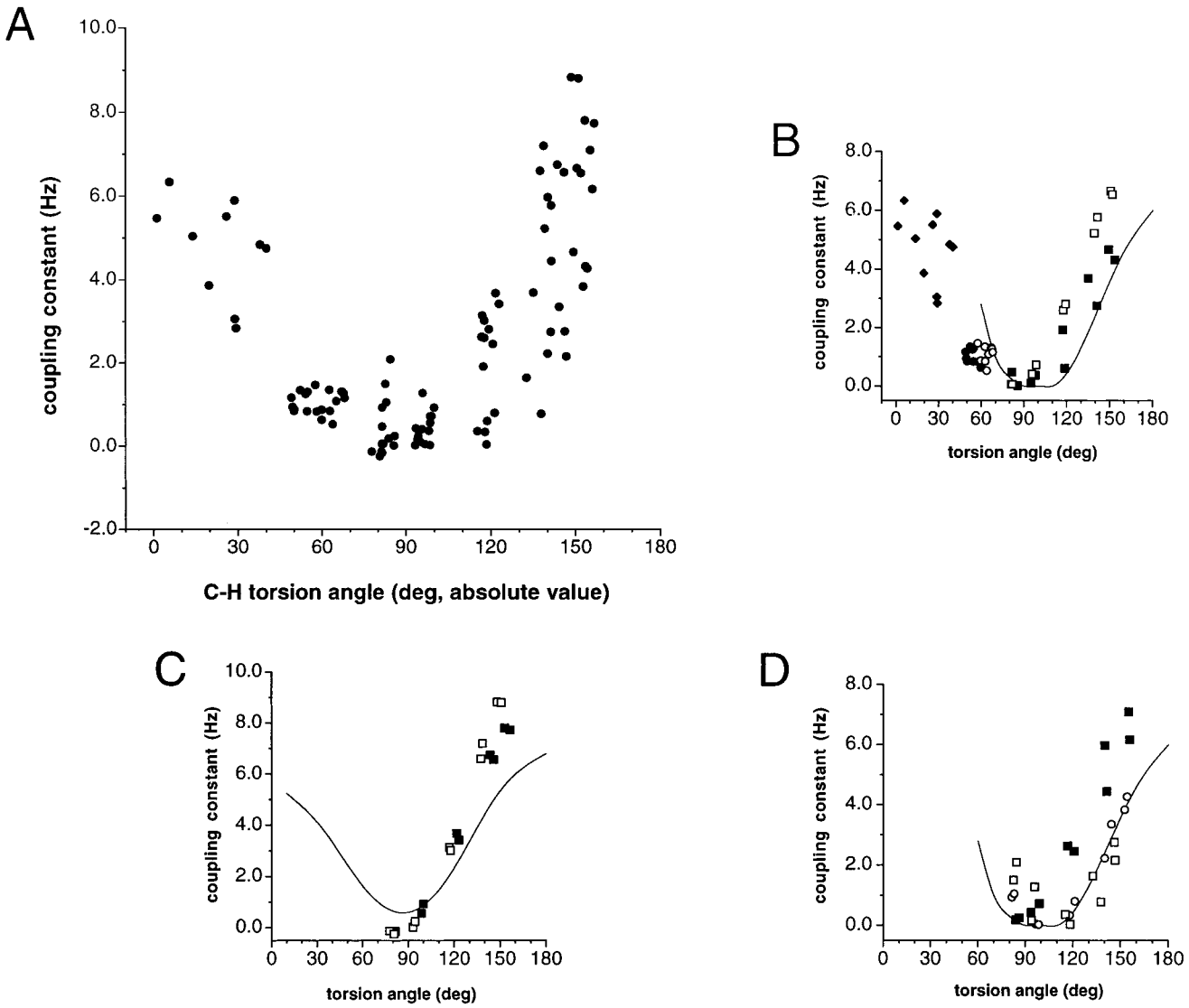

Figure 7. (A) Karplus curve derived from all computed $^3J_{CH}$ values in **1** using the DFT method (6-31G* basis set). (B) Karplus curve from computed $^3J_{CH}$ values in **1** pertaining to C−C−C−H coupling pathways. The solid line is the experimentally determined Karplus curve reported by Schwarcz and Perlin.[45] (C) Karplus curve from computed $^3J_{CH}$ values in **1** pertaining to C−O−C−H pathways ($^3J_{C1,H4}$, □; $^3J_{C4,H1}$, ■). The solid line is the experimentally determined Karplus curve reported by Tvaroska and co-workers.[47] (D) Karplus curve from computed $^3J_{CH}$ values in **1** pertaining to coupling pathways involving C2 and H2*R*/H2*S* of **1**. The solid line is the experimentally determined Karplus curve reported by Schwarcz and Perlin.[45] Absolute values of dihedral angles were used in each plot.

computed behavior (DFT) of $^2J_{C3,C5}$ confirms this prediction, with maximal coupling found at 1.3 P/π (10.4 Hz, ^{4}E) (Figure 9). Minimal coupling is predicted near ^{3}E, that is, in ring geometries where O3 is maximally out-of-plane. In all ring conformations, $^2J_{C3,C5}$ is positive, in agreement with the projection resultant rule.[51] However, the maximal value of $^2J_{C3,C5}$ predicted using the latter rule is 3−4 Hz (E_3/^{4}E forms, *gt* conformation about the C4−C5 bond), which is significantly lower than the DFT-calculated coupling. This difference may be due, in part, to limitations of the projection method, which was developed based on $^2J_{CC}$ values involving anomeric and secondary carbons appended with free hydroxyl groups.[51] In contrast, for $^2J_{C3,C5}$, a *terminal* coupled carbon is involved (C5), and C4 does not bear a free OH group but rather the ring oxygen. These differences may cause significant deviations in coupling behavior. The overall change in computed $^2J_{C3,C5}$ values with ring conformation (∼6.5 Hz) will probably be attenuated by rotation of the C4−C5 bond into the *gg* and *tg* conformations in solution where O5 is out-of-plane. In **2**, $^2J_{C3,C5}$ = 3.6 Hz, which is considerably smaller than the maximum coupling shown in Figure 9. This reduction is due to conformational averaging of the ring (60% E_2, 40% $^4T_3$) and about the C4−C5 bond (21% *gg*, 52% *gt*, 26% *tg*).[19] In the latter regard, $^2J_{C3,C5}$ values for *gg* and *tg* rotamers are expected to be small and possibly negative in sign, which would contribute to the smaller experimental $^2J_{C3,C5}$ value in **2**. In structures such as oligonucleotides where C4−C5 bond rotation is constrained (*gg*), differences in $^2J_{C3,C5}$ values between individual residues may prove more easily related to changes in ring conformation.

C. Three-Bond Couplings. Two $^3J_{CC}$ values exist in **1**, namely, $^3J_{C1,C5}$ and $^3J_{C2,C5}$. The magnitudes of these couplings depend, in part, on the C1−O4−C4−C5 and C2−C3−C4−C5 dihedral angles (Θ), respectively, which vary with ring conformation (data not shown; see Supporting Information). The torsion angles computed by the HF and DFT methods are virtually identical, and the computed dependencies of $^3J_{C1,C5}$ and $^3J_{C2,C5}$ on ring conformation (Figure 10A,B) determined by both methods are very similar. $^3J_{C1,C5}$ (DFT) varies from 0 to 4.5 Hz, with maximal coupling observed at ∼^{o}E and minimal coupling observed in the western hemisphere of the pseudorotational

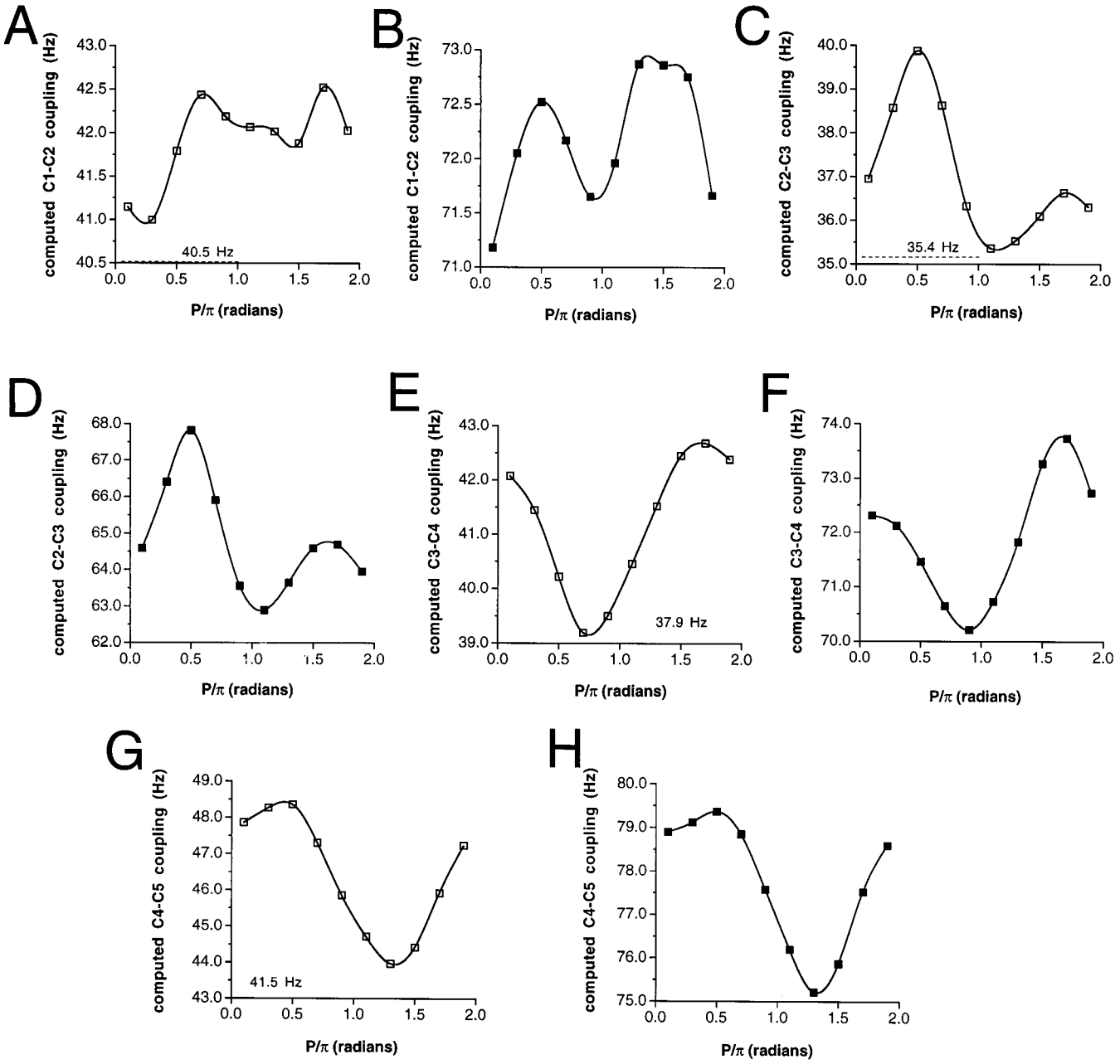

Figure 8. Computed $^1J_{CC}$ values in **1** as a function of ring conformation from DFT (UB3LYP/[5s2p1d|2s] and HF (UHF/[5s2p1d|2s]) methods using DFT (B3LYP/6-31G*) geometries: (A) $^1J_{C1,C2}$, DFT; (B) $^1J_{C1,C2}$, HF; (C) $^1J_{C2,C3}$, DFT; (D) $^1J_{C2,C3}$, HF; (E) $^1J_{C3,C4}$, DFT; (F) $^1J_{C3,C4}$, HF; (G) $^1J_{C4,C5}$, DFT; (H) $^1J_{C4,C5}$, HF.

itinerary. In contrast, $^3J_{C2,C5}$ (DFT) shows a maximal coupling near E_4 (3.7 Hz) and a minimal coupling near E_3 (~0 Hz). Amplitudes of the two curves differ, with $^3J_{C1,C5}$ showing larger maximal couplings than $^3J_{C2,C5}$. A plot of dihedral angle versus $^3J_{CC}$ for both $^3J_{C1,C5}$ and $^3J_{C2,C5}$ shows that both couplings exhibit a similar dependence on dihedral angle, with minimal coupling (~0 Hz) observed at $\Theta = 90°$ and maximal couplings of 4.0−5.0 Hz observed for $\Theta = \sim 180°$ (Figure 10C). The $^3J_{C1,C5}$ results are consistent with observed $^3J_{C1,C6}$ values in β-D-aldohexopyranosyl rings, which exhibit values of 4.0 ± 0.4 Hz[50,52−54] for C−O−C−C dihedral angles of ~180°. The C1−O4−C4−C5 pathway giving maximal Θ (162°, ^{o}E) resembles the C1−O5−C5−C6 pathway in β-D-aldohexopyranosyl rings since, in both pathways, O1 lies in the C−O−C−C coupling plane. The latter geometric factor is a major determinant of $^3J_{COCC}$ magnitude.[52,53] It should also be appreciated that C4−C5 bond rotation influences the magnitudes of $^3J_{C1,C5}$ and

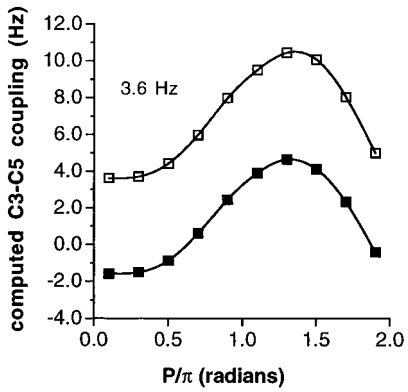

Figure 9. Computed $^2J_{C3,C5}$ values in **1** as a function of ring conformation using the DFT (□) and HF (■) methods ([5s2p1d|2s] basis set) at the B3LYP/6-31G* geometries. The indicated coupling is the observed $^2J_{C3,C5}$ value in **2**.

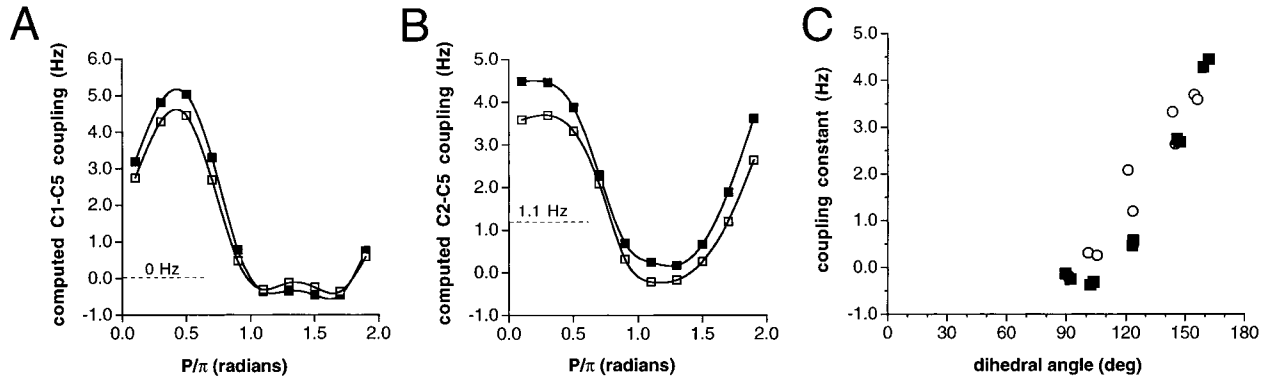

Figure 10. Computed $^3J_{CC}$ values in **1** as a function of ring conformation determined by the HF (closed symbols) and DFT (open symbols) methods ([5s2p1d|2s] basis set) at B3LYP/6-31G* geometries: (A) $^3J_{C1,C5}$; (B) $^3J_{C2,C5}$. The dotted lines and accompanying values are the corresponding experimental $^3J_{CC}$ values observed in **2**. (C) Partial Karplus curve derived from all computed $^3J_{CC}$ values in **1** using the DFT method ([5s2p1d|2s] basis set) at B3LYP/6-31G* geometries: $^3J_{C1,C5}$, ■; $^3J_{C2,C5}$, ○.

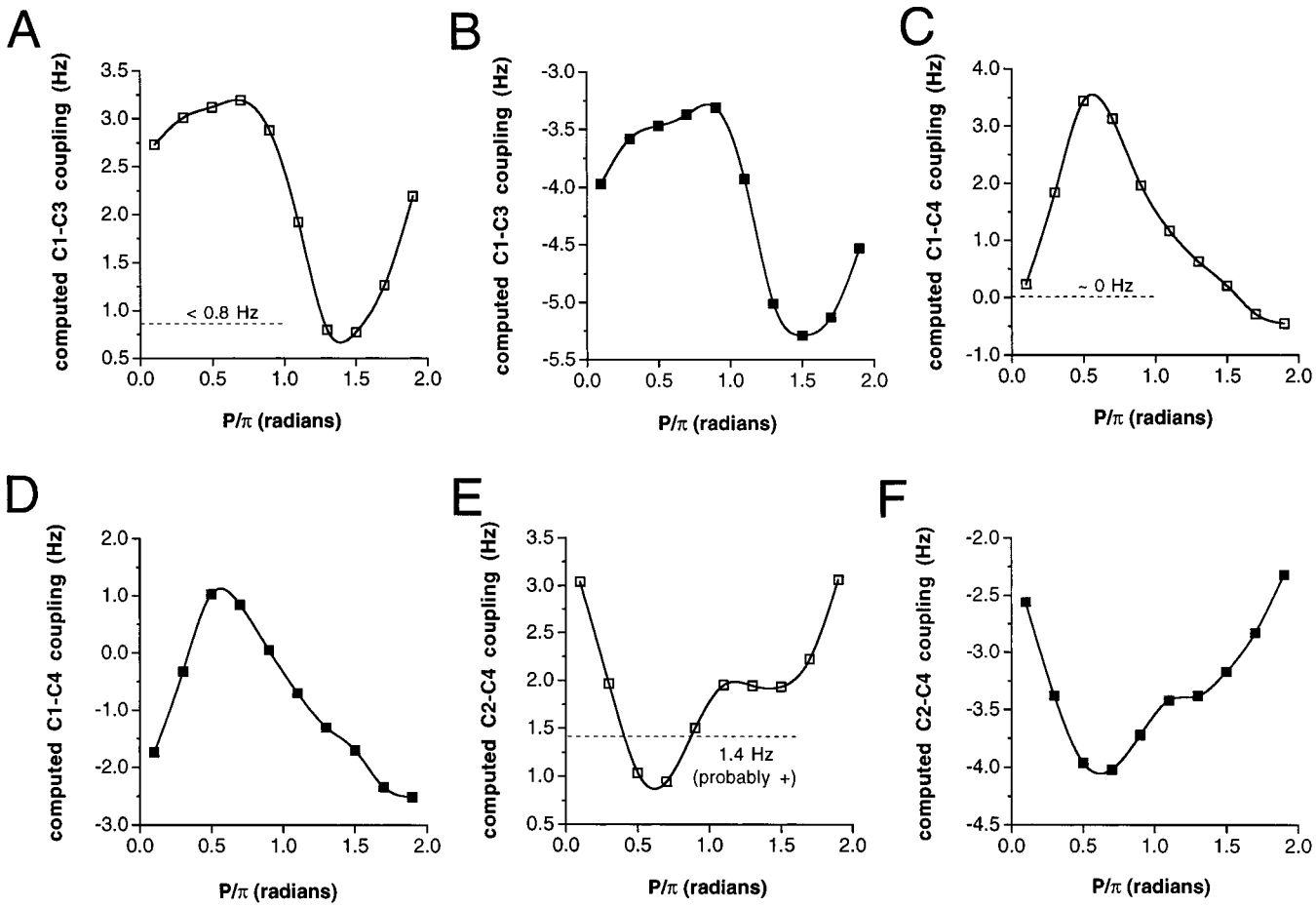

Figure 11. Computed $^{2+3}J_{CC}$ values in **1** as a function of ring conformation using the HF (closed symbols) and DFT (open symbols) method ([5s2p1d|2s] basis set) at B3LYP/6-31G* geometries: (A) $^{2+3}J_{C1,C3}$, DFT; (B) $^{2+3}J_{C1,C3}$, HF; (C) $^{2+3}J_{C1,C4}$, DFT; (D) $^{2+3}J_{C1,C4}$, HF; (E) $^{2+3}J_{C2,C4}$, DFT; (F) $^{2+3}J_{C2,C4}$, HF. The dotted lines and accompanying values are the corresponding experimental $^{2+3}J_{CC}$ values observed in **2**.

$^3J_{C2,C5}$.[53] In the present calculations, the C4−C5 bond is in the *gt* conformation and thus O5 cannot lie in the C1−O4−C4−C5 plane in any ring conformation, but coplanarity is possible for the C2−C3−C4−C5 pathway in ring geometries near ^{3}E. The latter arrangement is expected to *enhance* the observed sensitivity of $^3J_{C2,C5}$ to ring conformation; that is, the amplitude of the $^3J_{C2,C5}$ versus conformation curve may be smaller in the *gg* and *tg* rotamers; likewise, the amplitude of the $^3J_{C1,C5}$ curve may be greater in the *tg* rotamer.

D. Dual-Pathway Couplings. Couplings between C1 and C3, C1 and C4, and C2 and C4 in aldofuranosyl rings are governed by two intraring coupling pathways, and their magnitudes are expected to be determined by the algebraic sum of the couplings arising from both pathways.[54] These couplings, denoted as $^{2+3}J_{C1,C3}$, $^{2+3}J_{C1,C4}$, and $^{2+3}J_{C2,C4}$, are difficult to interpret in the absence of magnitude and sign information for both constituent pathways. The computed dependencies of these dual-pathway couplings on ring conformation are shown in Figure 11. The DFT-derived couplings are in closer agreement with experimental couplings observed in **2** than are HF-derived values, but coupling trends predicted by both methods are similar. $^{2+3}J_{C1,C3}$ values (DFT) vary from 0.8 to 3.2 Hz, with maximal coupling observed in conformers near E_1 and minimal couplings observed near E_o. $^{2+3}J_{C1,C4}$ varies from ∼0 to 3.4 Hz and exhibits maximal

coupling near ^{o}E and minimal coupling near E_2, while $^{2+3}J_{C2,C4}$ varies from 0.9 to 3.1 Hz, with maximal coupling observed near E_2 and minimal coupling observed near ^{o}E. All three dual-pathway couplings are predicted to be positive in sign, although small negative couplings are observed for $^{2+3}J_{C1,C4}$ in ^{1}E and E_2 conformers.

These dual-pathway couplings show a limited sensitivity to ring conformation, with the largest sensitivity exhibited by $^{2+3}J_{C1,C4}$ (>3.4 Hz). These dependencies can be used to test the behavior of their constituent $^{2}J_{CC}$ and $^{3}J_{CC}$ values if some assumptions are made. For example, $^{2+3}J_{C1,C4}$ is 3.4 Hz in ^{o}E and 0.2 Hz in E_o. In these two conformations, the C1−C2−C3−C4 dihedral angle is nearly constant at ∼0°. If the $^{3}J_{CCCC}$ contribution to both computed couplings is assumed to be constant (i.e., the ^{3}J component is relatively insensitive to the changes in orientation experienced by the terminal substituents), then the difference in the couplings (3.4 Hz − 0.2 Hz = 3.2 Hz) can be related to the $^{2}J_{COC}$ pathway. Thus, the two-bond C−O−C coupling must be *more negative* in the E_o conformer than in ^{o}E, assuming that the $^{3}J_{CCCC}$ pathways yield couplings having positive signs; the latter has been recently verified experimentally.[55] This prediction is consistent with experimental observations in D-aldohexopyranosyl rings. In α-anomers, $^{2}J_{C1,C5} = \sim -2$ Hz, whereas in β-anomers, $^{2}J_{C1,C5} = \sim 0$ Hz. The E_o conformer of **1** contains a C1−O4−C4 fragment resembling the C1−O5−C5 fragment in α-D-aldohexopyranosyl rings, and thus a ∼ −2 Hz coupling for the C1−O4−C4 pathway is expected. In contrast, the ^{o}E conformation contains a C1−O4−C4 fragment resembling the C1−O5−C5 fragment of β-D-aldohexopyranosyl rings, and a very small $^{2}J_{C1,C4}$ is expected. Given the approximations and assumptions in this analysis, the apparent agreement between calculated and experimental coupling behavior is reassuring.

A similar approach may be applied to analyze $^{2+3}J_{C1,C3}$ values. Again, we consider those conformations where the C3−C4−O4−C1 dihedral angle is ∼0°, namely, ^{2}E and E_2. Calculated couplings in these conformers are 2.9 and 2.2 Hz, respectively. Using the same rationale as above, we conclude that the two different *two-bond* pathways produce couplings that differ by ∼0.7 Hz; that is, $^{2}J_{C1,C3}$ values are very similar in the ^{2}E and E_2 conformers. This conclusion is consistent with prior observations on the behavior of $^{2}J_{CCC}$ values in carbohydrates.[51] Furthermore, in $^{2}E/E_2$ conformations, $^{2}J_{C1,C3}$ is probably negative in sign (−1−2 Hz) based on the application of the projection resultant method.[51] This prediction leads to a coupling of +3−5 Hz for the C1−O4−C4−C3 pathway, which is in qualitative agreement with recent studies of the dependency of $^{3}J_{COCC}$ values on dihedral angle in saccharides.[53]

Accuracy of DFT-Computed Coupling Constants. The utility of computed coupling constants in conformational analyses of carbohydrate structures such as **1** depends not only on their reliability in terms of predicting coupling trends but also on the extent to which they can be considered quantitative. Recent studies[19] have shown that HF-computed J_{CH} values in **1** are highly overestimated, and a similar overestimation is observed for J_{CC} (see Figure 8). Clearly correlation corrections are of paramount importance. In recent reports,[18,19,36] appropriate scaling factors were determined for J_{CH} values by computing specific spin couplings at a high level of theory, namely, quadratic configuration interaction (QCISD), and determining the scale factor which, when applied to the approximate correlation correction derived as the difference between MP2 calculations and the raw HF-calculated results, gave couplings identical to the QCISD values. The numerical values of the scaling factors depend on the coupling type; for example, scaling factors of 0.83, 0.75, and 0.83 were reported for $^{1}J_{CH}$, $^{2}J_{CH}$, and $^{3}J_{CH}$, respectively.[18,19,36] The scaled HF-derived J_{CH} values for **1** used in this manuscript were obtained in this fashion, whereas the DFT-derived J_{CH} values *were not scaled*. The level of agreement between the *scaled* HF and *unscaled* (raw) DFT couplings is remarkable, showing that the DFT treatment yields J_{CH} values (and presumably J_{CC} values) in closer agreement with the results of higher-level calculations *without the need for scaling*.

The extent of the difference between raw HF- and DFT-derived couplings can be observed in Figure 8. For example, $^{1}J_{C2,C3}$ values in **1** range from 63 to 68 Hz in the *unscaled* HF treatment, whereas the DFT results (also unscaled) yield a range of 35−40 Hz. The latter range is more consistent with the observed coupling of 35.4 Hz in **2**.

The true extent to which the scaled HF or unscaled DFT couplings agree with experimental data cannot be rigorously assessed, however, in structures such as **1** and **2** due to their inherent conformational flexibility. While many of the observed J_{CH} and J_{CC} values lie within the allowed ranges of the computed couplings, at least for the DFT method, these data are insufficient to address the question of accuracy unless a conformational model, itself subject to error, is invoked. We therefore conducted spin coupling calculations on the model methyl aldopyranoside (**3**) (optimized exocyclic torsions: O5−C1−O1−CH_3 = −68.9°; O5−C5−C6−O6 = 71.0° (*gt* conformer); C5−C6−O6−H = −169.6°; C1−C2−O2−H = 177.0°). Five J_{CH} values in **3** were calculated (DFT), giving the following results: $^{1}J_{C1,H1}$ = 152.7 Hz; $^{2}J_{C1,H2}$ = −6.1 Hz; $^{2}J_{C1,H5}$ = 2.2 Hz; $^{3}J_{C1,H3R}$ = 2.3 Hz; $^{3}J_{C1,H3S}$ = 7.8 Hz. These computed couplings were compared to those observed in methyl β-D-glucopyranoside (**4**), which has a similar structure to **3**: $^{1}J_{C1,H1}$ = 161.3 Hz; $^{2}J_{C1,H2}$ = −6.3 Hz; $^{2}J_{C1,H5}$ = 2.3 Hz. These results show the DFT-computed $^{1}J_{CH}$ value to be 5.6% lower (absolute error of 8.6 Hz), in good agreement with the error estimates made above for $^{1}J_{CH}$ values in **1**. The computed $^{2}J_{CH}$ and $^{3}J_{CH}$ values appear to contain similar percent errors, which translate into smaller absolute errors (∼0.2 Hz for $^{2}J_{C1,H2}$, ∼0.1 Hz for $^{2}J_{C1,H5}$). The negative sign of $^{2}J_{C1,H2}$ is accurately predicted by the computations. Interestingly, $^{3}J_{C1,H3R}$ = 2.3 Hz in **3**, but $^{3}J_{C1,H3}$ = 1.2 Hz in **4**; likewise, $^{3}J_{C1,H3S}$ = 7.8 Hz in **3**, but $^{3}J_{C1,H3}$ = 6.0 Hz in methyl β-D-allopyranoside (**5**) in which H3 is equatorial. The smaller couplings in **4** and **5** compared to the computed values are caused by the different substitution pattern at C3; loss of an electronegative substituent on the carbon bearing the coupled proton apparently makes a positive contribution to $^{3}J_{CCCH}$ values.

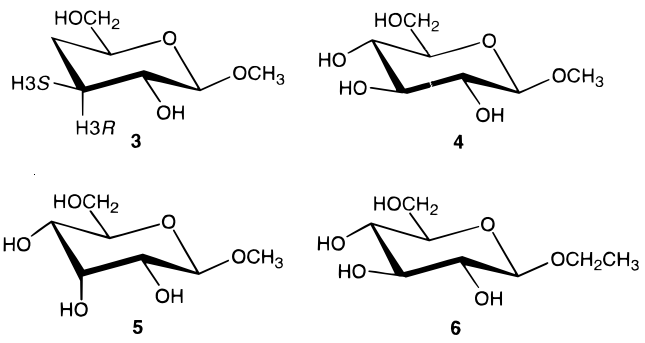

J_{CC} values were also computed in **3** and compared to corresponding experimental values in ethyl β-D-glucopyranoside (**6**). Computed couplings in **3** were $^{1}J_{C1,C2}$ = 53.6 Hz, $^{2}J_{C1,C3}$ = 1.4

Hz, $^2J_{C1,C5} = -1.2$ Hz, $^3J_{C1,C6} = 4.0$ Hz, and $^2J_{C1,CH3} = -2.2$ Hz. By comparison, in **6**, $^1J_{C1,C2} = 46.9$ Hz, $^2J_{C1,C3} = +4.5$ Hz, $^2J_{C1,C5} = \sim 0$ Hz, $^3J_{C1,C6} = 4.1$ Hz, and $^2J_{C1,CH3} = -1.8$ Hz. In contrast to observations on J_{CH}, computed J_{CC} values appear *larger* than experimental values; for $^1J_{C1,C2}$ and $^2J_{C1,CH3}$, the percent increases are ~13% and ~18%, respectively, although the error in the latter is greater due to the small magnitude of $^2J_{C1,CH3}$ and the error associated with its measurement (±0.1 Hz). It is important to note, however, that $^1J_{C1,C2}$ is affected significantly by the particular selection of C1−O1 and C2−O2 torsions, which in the present case orient the aglycone CH_3 and OH-2 *anti* to C2 and C1, respectively. These orientations are expected to give rise to a maximal or near-maximal value of $^1J_{C1,C2}$.[49] If either of these torsions is rotated to a *gauche* orientation, the computed $^1J_{C1,C2}$ decreases by 4−6 Hz. A simple Boltzmann average, weighted by the optimized energies in the various rotamers, yielded a value of 47.8 Hz for $^1J_{C1,C2}$, which is in closer agreement with the observed coupling of 46.9 Hz. Comparisons for $^2J_{C1,C5}$ and $^3J_{C1,C6}$ between **3** and **6** are less reliable due to the conformational flexibility of the C5−C6 bond of **6** in solution. Overall, the level of agreement between experiment and theory is remarkable, leading to the expectation that DFT-derived J_{CH} and J_{CC} values will provide a useful means of testing structure-coupling correlations in situations not readily studied via experiment.

The above comparison is not without limitations in that only one set of exocyclic torsion angles was inspected in **3**, whereas conformational averaging about these bonds is expected in solutions of **4**−**6**. The effect of this averaging on computed *J* values remains largely unknown. However, this uncertainty notwithstanding, the available data suggest that J_{CH} and J_{CC} values computed by the DFT method are 5−6% smaller and ~5−10% larger, respectively, than experimental values. Knowledge of these correction factors may permit the quantitative use of these couplings in future structural studies of saccharides. Improved basis sets in the geometry optimization and *J* coupling calculations, and an accounting of non-Fermi-contact terms in the latter, may further improve the agreement between theory and experiment.

Conclusions

This investigation has provided a detailed comparison of structural parameters (bond lengths, bond angles, bond torsions) and NMR spin coupling constants (J_{CH} and J_{CC}) in a biologically important aldopentofuranose, 2-deoxy-*β*-D-*erythro*-pentofuranose (**1**), obtained by two different computational methods: ab initio self-consistent field Hartree−Fock calculations and density functional calculations, both using the same basis sets (6-31G* for geometry optimization and [5s2p1d|2s] for coupling constant evaluation). The primary aim was to evaluate the DFT method as applied to carbohydrate systems with respect to its ability to compute NMR scalar couplings involving carbon. Previous efforts to calculate *J* values in **1** using HF-based methods,[19] while useful, were nevertheless cumbersome, requiring both HF and MP2 calculations and the development of scaling factors (from QCISD calculations on structurally related but smaller systems) to moderate the overestimation of electron correlation effects on the computed couplings in the MP2 calculations. The DFT approach, which is designed to recover the important effects of electron correlation, was expected to yield reliable *J* values directly, that is, computed values that do not require scaling. This expectation has been realized. While structural parameters, especially bond lengths, clearly differ in the HF and DFT treatments, the *scaled* HF and *unscaled* DFT couplings are in very good agreement with respect to both coupling trends and absolute values. Thus, the DFT method provides a simpler, more rapid approach to computing *J* couplings than the scaling approach based on both HF and MP2 values, with comparable accuracy. This observation provides a firm foundation for the application of the DFT method to larger carbohydrates such as oligosaccharides, where J_{CH} and J_{CC} values, especially those across the *O*-glycosidic linkages, can be investigated more thoroughly as potential probes of conformation in solution.[53] It should be noted that the DFT method can also be used to compute $^3J_{HH}$ values, which may provide new insights into torsional and nontorsional (e.g., Barfield effects) factors that influence these couplings in cyclic systems such as furanosyl rings.

While the high level of agreeement between the scaled HF and unscaled DFT results for **1** is encouraging, the DFT-derived *J* values cannot yet be considered quantitative. We estimate that, using the DFT approach described herein, the computed J_{CH} and J_{CC} values are 5−6% *smaller* and ~5−10% *larger*, respectively, than experimental values. Interestingly, although different calculational methods were employed, Hricovini et al.[23c] estimated errors of ~5% in recent DFT calculations of J_{CH} values in methyl *β*-D-xylopyranoside, again with calculated couplings smaller than experimental couplings. The origin of these deviations has not yet been identified but could stem from the inherent limitations of the calculations (e.g., choice of basis set, limitation of the calculations to one set of exocyclic torsions in **1**, and others) as well as from the neglect of non-Fermi-contact terms in the calculations. It would be desirable to identify the cause(s) of these relatively small discrepancies between theory and experiment and correct them in order to establish a firm computational method for the quantitative prediction of J_{CH} and J_{CC} in carbohydrates, which would stimulate their wider application in structural studies. Despite these current limitations, however, the robustness of the DFT approach is remarkable and worthy of further development and exploitation.

The effects of furanose ring conformation on J_{CC} values in **1** have been newly examined in this study. The computed behavior of $^2J_{C3,C5}$ in **1** is in qualitative agreement with predictions based on the projection resultant method,[51] thereby providing further evidence of the potential of this coupling as a conformational probe. Karplus curves constructed from DFT-computed $^3J_{CC}$ and $^3J_{CH}$ values in **1** are in good agreement with those derived previously from experiment,[45−48,53] thus providing evidence that the computed longer-range couplings are nearly quantitative. New insights into dual-pathway $^{2+3}J_{CC}$ values in **1** evolved from the calculation of these couplings as a function of ring conformation; these new data provide a means to dissect $^{2+3}J_{CC}$ values into their ^2J and ^3J components, at least for a few ring conformers. Overall, the results of this investigation provide a strong incentive to measure J_{CH} and J_{CC} in more complex furanose-containing biomolecules (e.g., DNA, RNA) where they may yield conformational information complementary to that provided by more common $^3J_{HH}$ and NOE measurements. The inclusion of J_{CH} and J_{CC} should be particularly beneficial in studies of conformationally flexible systems where the interpretation of more conventional NMR parameters such as NOE can sometimes be problematic.

Acknowledgment. This work was supported by a grant from Omicron Biochemicals, Inc., South Bend, IN, and by the Office of Basic Energy Sciences of the United States Department of Energy. This is Document No. NDRL-4085 from the Notre Dame Radiation Laboratory.

Supporting Information Available: Three figures of C−H bond lengths, C−O bond lengths, C−O torsions, puckering amplitude, and C4−O4−C1 bond angle in **1** as a function of ring conformation determined by the HF/6-31G* and B3LYP/6-31G* methods and three figures of C−H torsion angles, C−C bond lengths, and C1−C5 and C2−C5 torsion angles in **1** as a function of ring conformation determined by the B3LYP/6-31G* method. This material is available free of charge via the internet at http://pubs.acs.org.

References and Notes

(1) Karplus, M. *J. Chem. Phys.* **1959**, *30*, 11−15.

(2) Govil, G.; Hosur, R. V. *Conformation of Biological Molecules, NMR: Basic Principles and Progress*; Springer-Verlag: Berlin, 1982; Vol. 20, p 19.

(3) Bock, K.; Pedersen, C. *J. Chem. Soc., Perkin Trans. II* **1974**, 293−297.

(4) Bock, K.; Pedersen, C. *Acta Chem. Scand.* **1975**, *B29*, 258−264.

(5) (a) Bock, K.; Pedersen, C. *Acta Chem. Scand.* **1977**, *B31*, 354−358. (b) Schwarcz, J. A.; Cyr, N.; Perlin, A. S. *Can. J. Chem.* **1975**, *53*, 1872−1875.

(6) Tvaroska, I.; Taravel, F. R. *Carbohydr. Res.* **1991**, *221*, 83−94.

(7) Tvaroska, I.; Taravel, F. R. *J. Biomol. NMR* **1992**, *2*, 421−430.

(8) Hricovini, M.; Tvaroska, I. *Magn. Reson. Chem.* **1990**, *28*, 862−866.

(9) Egli, H.; von Philipsborn, W. *Helv. Chim. Acta* **1981**, *64*, 976−988.

(10) Mierke, D. F.; Grdadolnik, S. G.; Kessler, H. *J. Am. Chem. Soc.* **1992**, *114*, 8283−8284.

(11) Vuister, G. W.; Delaglio, F.; Bax, A. *J. Am. Chem. Soc.* **1992**, *114*, 9674−9675.

(12) Vuister, G. W.; Delaglio, F.; Bax, A. *J. Biomol. NMR* **1993**, *3*, 67−80.

(13) (a) Haasnoot, C. A. G.; de Leeuw, F. A. A. M.; Altona, C. *Tetrahedron* **1980**, *36*, 2783−2792. (b) Haasnoot, C. A. G.; de Leeuw, F. A. A. M.; de Leeuw, H. P. M.; Altona, C. *Org. Magn. Reson.* **1981**, *15*, 43−52. (c) Donders, L. A.; de Leeuw, F. A. A. M.; Altona, C. *Magn. Reson. Chem.* **1989**, *27*, 556−563. (d) Altona, C.; Ippel, J. H.; Westra Hoekzema, A. J. A.; Erkelens, C.; Groesbeek, M.; Donders, L. A. *Magn. Reson. Chem.* **1989**, *27*, 564−576.

(14) (a) Biamonti, C.; Rios, C. B.; Lyons, B. A.; Montelione, G. T. *Adv. Biophys. Chem.* **1994**, *4*, 51−120. (b) Eberstadt, M.; Gemmecker, G.; Mierke, D. F.; Kessler, H. *Angew. Chem., Int. Ed. Engl.* **1995**, *34*, 1671−1695.

(15) Otting, G.; Messerle, B. A.; Soler, L. P. *J. Am. Chem. Soc.* **1996**, *118*, 5096−5102.

(16) Jardetzky, O. *Biochim. Biophys. Acta* **1980**, *621*, 227−232.

(17) Homans, S. W. *Prog. NMR Spectrosc.* **1990**, *22*, 1−53.

(18) Podlasek, C. A.; Stripe, W. A.; Carmichael, I.; Shang, M.; Basu, B.; Serianni, A. S. *J. Am. Chem. Soc.* **1996**, *118*, 1413−1425.

(19) Church, T. J.; Carmichael, I.; Serianni, A. S. *J. Am. Chem. Soc.* **1997**, *119*, 8946−8964.

(20) Carmichael, I. *J. Phys. Chem.* **1993**, *97*, 1789−1792.

(21) Serianni, A. S.; Wu, J.; Carmichael, I. *J. Am. Chem. Soc.* **1995**, *117*, 8645−8650.

(22) Bauschlicher, C. W., Jr.; Partridge, H. *Chem. Phys. Lett.* **1995**, *240*, 533−40.

(23) (a) Malkin, V. G.; Malkina, O. L.; Eriksson, L. A.; Salahub, D. R. In *The calculation of NMR and ESR spectroscopy parameters using density functional theory*; Malkin, V. G., Malkina, O. L., Eriksson, L. A., Salahub, D. R., Eds.; Elsevier Science B.V.: Amsterdam, 1995; Vol. 2, pp 273−347. (b) Stahl, M.; Schopfer, U.; Frenking, G.; Hoffmann, R. W. *J. Org. Chem.* **1997**, *62*, 3702−3704. (c) Hricovini, M.; Malkina, O. L.; Bizik, F.; Nagy, L. T.; Malkin, V. G. *J. Phys. Chem. A* **1997**, *101*, 9756−9762.

(24) Frisch, M. J.; Trucks, G. W.; Schlegel, H. B.; Gill, P. M. W.; Johnson, B. G.; Robb, M. A.; Cheeseman, J. R.; Keith, T.; Petersson, G. A.; Montgomery, J. A.; Raghavachari, K.; Al-Laham, M. A.; Zakrzewski, V. G.; Ortiz, J. V.; Foresman, J. B.; Peng, C. Y.; Ayala, P. Y.; Chen, W.; Wong, M. W.; Andres, J. L.; Replogle, E. S.; Gomperts, R.; Martin, R. L.; Fox, D. J.; Binkley, J. S.; Defrees, D. J.; Baker, J.; Stewart, J. P.; Head-Gordon, M.; Gonzalez, C.; Pople, J. A. *Gaussian 94*, Revision B.3; Gaussian, Inc.: Pittsburgh, PA, 1995.

(25) Becke, A. D. *J. Chem. Phys.* **1993**, *98*, 5648−5652.

(26) Slater, J. C. *The Self-Consistent Field for Molecules and Solids*; McGraw-Hill: New York, 1974.

(27) Becke, A. D. *ACS Symp. Ser.* **1989**, *394*, 165.

(28) Vosko, S. H.; Wilk, L.; Nusair, M. *Can. J. Phys.* **1980**, *58*, 1200−1211.

(29) Lee, C.; Yang, W.; Parr, R. G. *Phys. Rev. B* **1988**, *37*, 785.

(30) Barone, V. *J. Chem. Phys.* **1994**, *101*, 6834−6838.

(31) Lemieux, R. U.; Koto, S. *Tetrahedron* **1974**, *30*, 1933−1944.

(32) Praly, J.-P.; Lemieux, R. U. *Can. J. Chem.* **1987**, *65*, 213−223.

(33) Lemieux, R. U. *Pure Appl. Chem.* **1971**, *25*, 527−548.

(34) Kowalewski, J.; Laaksonen, A.; Roos, B.; Siegbahn, P. *J. Chem. Phys.* **1979**, *71*, 2896−2902.

(35) Hehre, W. J.; Radom, L.; Schleyer, P. v. R.; Pople, J. A. *Ab initio Molecular Orbital Theory*; Wiley-Interscience: New York, 1985.

(36) Serianni, A. S.; Wu, J.; Carmichael, I. *J. Am. Chem. Soc.* **1995**, *117*, 8645−8650.

(37) Serianni, A. S.; Chipman, D. M. *J. Am. Chem. Soc.* **1987**, *109*, 5297−5303.

(38) Garrett, E. C.; Serianni, A. S. *Carbohydr. Res.* **1990**, *206*, 183−191.

(39) Juaristi, E.; Cuevas, G. *The Anomeric Effect*; CRC Press: Boca Raton, FL, 1995.

(40) Cossé-Barbi, A.; Dubois, J.-E. *J. Am. Chem. Soc.* **1987**, *109*, 1503−1511.

(41) Serianni, A. S.; Barker, R. *J. Org. Chem.* **1984**, *49*, 3292−3300.

(42) Hines, J. V.; Varani, G.; Landry, S. M.; Tinoco, I., Jr. *J. Am. Chem. Soc.* **1993**, *115*, 11002−11003.

(43) Marino, J. P.; Schwalbe, H.; Glaser, S. J.; Griesinger, C. *J. Am. Chem. Soc.* **1996**, *118*, 4388−4395.

(44) Podlasek, C. A.; Wu, J.; Stripe, W. A.; Bondo, P. B.; Serianni, A. S. *J. Am. Chem. Soc.* **1995**, *117*, 8635−8644.

(45) Schwarcz, J. A.; Perlin, A. S. *Can. J. Chem.* **1972**, *50*, 3667−3676.

(46) Spoormaker, T.; de Bie, M. J. A. *Recl. Trav. Chim. Pays-Bas* **1978**, *97*, 85−87.

(47) Tvaroska, I.; Hricovini, H.; Petrakova, E. *Carbohydr. Res.* **1989**, *189*, 359−362.

(48) Mulloy, B.; Frenkiel, T. A.; Davies, D. B. *Carbohydr. Res.* **1988**, *184*, 39−46.

(49) Carmichael, I.; Chipman, D. M.; Podlasek, C. A.; Serianni, A. S. *J. Am. Chem. Soc.* **1993**, *115*, 10863−10870.

(50) Wu, J.; Bondo, P. B.; Vuorinen, T.; Serianni, A. S. *J. Am. Chem. Soc.* **1992**, *114*, 3499−3505.

(51) Church, T.; Carmichael, I.; Serianni, A. S. *Carbohydr. Res.* **1996**, *280*, 177−186.

(52) King-Morris, M. J.; Serianni, A. S. *J. Am. Chem. Soc.* **1987**, *109*, 3501−3508.

(53) Bose, B.; Zhao, S.; Stenutz, R.; Cloran, F.; Bondo, P. B.; Bondo, G.; Hertz, B.; Carmichael, I.; Serianni, A. S. *J. Am. Chem. Soc.* **1998**, *120*, 11158−11173.

(54) Marshall, J. L. *Carbon−Carbon and Carbon-Proton NMR Couplings: Applications to Organic Stereochemistry and Conformational Analysis, Methods in Stereochemical Analysis*; Verlag Chemie International: Deerfield Beach, FL, 1983; Vol. 2, pp 186−193.

(55) Serianni, A. S.; Bondo, P. B.; Zajicek, J. *J. Magn. Reson. Ser. B* **1996**, *112*, 69−74.